Bound states and decay times of fermions in a Schwarzschild black hole background

Anthony Lasenby,* Chris Doran,† Jonathan Pritchard, Alejandro Caceres, and Sam Dolan
Astrophysics Group, Cavendish Laboratory, Madingley Road, Cambridge CB3 0HE, United Kingdom
(Received 2 March 2005; published 22 November 2005)

We compute the spectrum of normalizable fermion bound states in a Schwarzschild black hole background. The eigenstates have complex energies. The real parts of the energies, for small couplings, closely follow a hydrogenlike spectrum. The imaginary parts give decay times for the various states, due to the absorption properties of the hole, with states closer to the hole having shorter half-lives. As the coupling increases, the spectrum departs from that of the hydrogen atom, as states close to the horizon become unfavorable. Beyond a certain coupling the $1S_{1/2}$ state is no longer the ground state, which shifts to the $2P_{3/2}$ state, and then to states of successively greater angular momentum. For each positive energy state a negative energy counterpart exists, with opposite sign of its real energy, and the same decay factor. It follows that the Dirac sea of negative energy states is decaying, which may provide a physical contribution to Hawking radiation.

DOI: 10.1103/PhysRevD.72.105014 PACS numbers: 03.65.Ge, 03.65.Pm, 04.62.+v, 04.70.Bw

I. INTRODUCTION

Quantum theory in a black hole background has been extensively studied by many authors. Detailed discussions of this problem are contained in the books by Birrell and Davies [1] and Chandrasekhar [2], and the review paper by Brout *et al.* [3]. Much of the attention in this work is focused on the wave equation and its scattering properties. Detailed studies of the Dirac equation in a black hole background are less common. Indeed, the lowest order scattering cross section for a fermion in a black hole background has only recently been computed [4–6]. In this paper we investigate another previously neglected aspect of quantum mechanics in a black hole background. This is the existence of the bound state spectrum for particles orbiting a spherically symmetric point source. That is, we study the gravitational analog of the hydrogen atom orbitals.

There has been strangely little effort devoted to the study of the bound state spectrum, despite the fundamental importance of the electromagnetic analog. But it is clear that these states must exist—how else can one provide a quantum description of a particle in orbit around a black hole? These states must also be essential in the quantum description of the capture process. The problem was discussed in 1974 by Deruelle and Ruffini [7], who described the existence of resonance states in the Klein-Gordon equation. Further significant contributions were made in a series of papers by Gaina and coauthors [8–10]. These papers give various analytic expressions for the real and imaginary parts of the energy in a series of limiting cases.

Much of the study of quantum mechanics in a black hole background has focused on the related, though distinct, problem of finding the quasinormal mode spectrum. Quasinormal modes are purely ingoing at the horizon, and outgoing at infinity[2]. These boundary conditions produce a spectrum of eigenstates with complex-valued energies. The significance of these quasinormal modes comes from their use in describing black hole oscillations. But the boundary condition at infinity implies that these modes are not normalizable, so they cannot represent bound states. The problem of interest here is to find normalizable bound states, so we seek solutions that are purely ingoing at the horizon and fall off exponentially at infinity.

For a particle of mass m in the field of a black hole of mass M the dimensionless coupling strength is defined by

$$\alpha = \frac{mM}{m_p^2} \tag{1}$$

where m_p is the Planck mass. In this paper we compute the fermion bound state spectra for α in the range $0 \cdots 6$. If the bound particle is assumed to be an electron, this range corresponds to black holes of masses up to 1×10^{15} kg, which is the scale appropriate for primordial black holes formed in the early universe. Computing the energy spectrum is more complicated than the hydrogen atom case for two main reasons. The first is that the radially separated Dirac equation contains three singular points, only two of which are regular. There is no special function theory appropriate for the study of such equations, so we have to resort to a range of numerical techniques to find the spectrum. The second problem is that the singularity at the center of a Schwarzschild black hole acts as a current sink. All normalizable states must therefore decay in time, and we must search for eigenstates over the two-dimensional space of complex energies. The states we construct therefore all have a finite half-life, so they can be viewed as resonance states. The interpretation of these states is discussed in Sec. VIII.

Despite these difficulties, the problem can be tackled numerically, and we present a range of results for the real and imaginary parts of the energy. These are sufficient to

*Email address: a.n.lasenby@mrao.cam.ac.uk
†Email address: C.Doran@mrao.cam.ac.uk

predict how the spectrum will behave for larger values of the coupling constant. The first result, which is entirely to be expected, is that the orbitals become increasingly tightly bound as the coupling increases. It follows that, for a given state, the energy will initially decrease with α, but will eventually turn around and start increasing as the particle spends too much time inside the classical radius of minimum energy. States with higher angular momentum then become energetically favorable as α increases. For example, we show that beyond $\alpha \approx 0.6$ the $1S_{1/2}$ state is no longer the ground state. While the real part of the energy behaves in quite a complicated fashion, the imaginary part, which controls the decay rate, simply increases in magnitude. This is also as one would expect. The closer the orbital density is to the singularity, the greater the probability of capture.

We start by discussing the Dirac equation in a Schwarzschild background in an arbitrary gauge. This is helpful in establishing a range of gauge-invariant results. In particular, the energy conjugate to time translation symmetry is confirmed to be a gauge-invariant quantity. This is important in order to guarantee that the quantity is a physical observable. We next establish the behavior of the wave function around the horizon, which is sufficient to establish that the states must decay exponentially with time. We then turn to a specific choice of gauge that is well suited to a numerical solution. We solve the equations by simultaneously integrating out from the horizon and in from infinity. We then vary the energy to ensure that the solutions match at some finite radius. This process guarantees that we find a global, normalizable bound state. A set of spectra is obtained, and the density is plotted for a range of states. Decay rates and expectation values for the distance are also presented. We end with a discussion of the significance of these bound states, and the possible physical processes that they may generate. Except where stated otherwise, natural units with $G = \hbar = c = 1$ are assumed throughout. We employ a spacetime metric with signature -2.

II. COORDINATES AND TETRADS FOR THE SCHWARZSCHILD SOLUTION

We start by defining a general parametrization of the Schwarzschild solution. This general form will help to guarantee that various expressions are coordinate and gauge invariant. It is essential to our approach that we treat the horizon correctly. In particular, we are only interested in coordinate systems that are not singular there, so we cannot work with standard Schwarzschild coordinates. Two suitable systems are provided by advanced Eddington-Finkelstein coordinates,

$$ds^2 = (1 - 2M/r)dt^2 - (4M/r)dtdr - (1 + 2M/r)dr^2 - r^2(d\theta^2 + \sin^2\theta d\phi^2), \tag{2}$$

and Painlevé-Gullstrand coordinates [4,6],

$$ds^2 = (1 - 2M/r)dt^2 - \sqrt{8M/r}dtdr - dr^2 - r^2(d\theta^2 + \sin^2\theta d\phi^2). \tag{3}$$

In both of these line elements the r, θ, and ϕ coordinates are the same, taking the usual range for spherical polar coordinates, $0 \le r < \infty$, $0 \le \theta \le \pi$, and $0 \le \phi < 2\pi$. The time coordinate t is different in the two systems, but in both cases takes the range $-\infty < t < \infty$. Both coordinate systems deal smoothly with the horizon, and cover regions I and III of the Penrose diagram of the fully extended Kruskal manifold [1]. These two regions are the ones of physical relevance for this paper.

In order to formulate the Dirac equation in a gravitational background it is necessary to first introduce a tetrad. With Greek letters referring to the coordinate basis, and Latin letters referring to the orthonormal basis, a suitable tetrad for both of the preceding coordinate systems can be written in the form

$$e_\mu{}^a = \begin{pmatrix} a_1 & a_2 & 0 & 0 \\ b_2 & b_1 & 0 & 0 \\ 0 & 0 & 1/r & 0 \\ 0 & 0 & 0 & 1/r\sin\theta \end{pmatrix}. \tag{4}$$

Here a_1, a_2, b_1, b_2 are scalar functions of r satisfying

$$a_1 b_1 - a_2 b_2 = 1, \qquad (b_1)^2 - (b_2)^2 = 1 - 2M/r. \tag{5}$$

As a consequence of these relations we find that we can also write

$$e^\mu{}_a = \begin{pmatrix} b_1 & -b_2 & 0 & 0 \\ -a_2 & a_1 & 0 & 0 \\ 0 & 0 & r & 0 \\ 0 & 0 & 0 & r\sin\theta \end{pmatrix}. \tag{6}$$

Explicitly, for advanced Eddington-Finkelstein coordinates we can set

$$\begin{aligned} a_1 &= 1 + M/r, \qquad a_2 = M/r, \\ b_1 &= 1 - M/r, \qquad b_2 = -M/r, \end{aligned} \tag{7}$$

and for Painlevé-Gullstrand coordinates we can work with the ''Newtonian'' choice [4,11] which sets

$$a_1 = 1, \qquad a_2 = 0, \qquad b_1 = 1, \qquad b_2 = -(2M/r)^{1/2}. \tag{8}$$

The general line element generated by the tetrad of Eq. (4), subject to conditions (5) is

$$g_{\mu\nu}dx^\mu dx^\nu = (1 - 2M/r)dt^2 + 2(a_1 b_2 - a_2 b_1)dtdr - ((a_1)^2 - (a_2)^2)dr^2 - r^2(d\theta^2 + \sin^2\theta d\phi^2). \tag{9}$$

Any four functions a_1, a_2, b_1, b_2 satisfying Eqs. (5) generate a line element that represents the Schwarzschild

solution. It may appear that the line element (9) contains two coefficients that we can choose arbitrarily, but in fact the terms are related by

$$(1 - 2M/r)((a_1)^2 - (a_2)^2) + (a_1 b_2 - a_2 b_1)^2 = 1. \quad (10)$$

One way in which we can alter the coefficients in the line element (9) is by transforming the time coordinate through the addition of an arbitrary radially dependent term. That is, we can set

$$\bar{t} = t + \alpha(r), \quad (11)$$

and the new line element will be independent of the new time coordinate $\bar{t}$. Rather than think in terms of changing the time coordinate, however, it is simpler for our purposes to always label the time coordinate as t and instead redefine a_1 and a_2. These then transform as

$$a_1 \mapsto \bar{a}_1 = a_1 - b_2 \alpha', \qquad a_2 \mapsto \bar{a}_2 = a_2 - b_1 \alpha', \quad (12)$$

with b_1 and b_2 unchanged. Throughout primes denote derivatives with respect to r. It is straightforward to confirm that the new set $(\bar{a}_1, \bar{a}_2, b_1, b_2)$ still satisfy the constraints of Eq. (5). In order for the new a_1 and a_2 functions to be well defined, it is necessary that α be continuous.

The four variables a_1, a_2, b_1 and b_2 are subject to two constraint equations, so they must contain two arbitrary degrees of freedom. The first arises from the freedom in the time coordinate as described in Eq. (12). The second lies in the freedom to perform a radially dependent boost of the tetrad frame, which transforms the variables according to

$$\begin{pmatrix} a_1 & b_1 \\ a_2 & b_2 \end{pmatrix} \mapsto \begin{pmatrix} \cosh\beta & \sinh\beta \\ \sinh\beta & \cosh\beta \end{pmatrix} \begin{pmatrix} a_1 & b_1 \\ a_2 & b_2 \end{pmatrix} \quad (13)$$

where β is an arbitrary, nonsingular function of r. This boost does not alter the line element of Eq. (9).

Outside the horizon we have $|b_1| > |b_2|$, and in the asymptotically flat region b_1 can be brought to $+1$ by a suitable boost. It follows that we must have

$$b_1 > 0 \quad \forall \; r \geq 2M. \quad (14)$$

At the horizon we therefore have b_1 positive, and $b_2 = \pm b_1$. For black holes the negative sign is the correct one, as this choice guarantees that all particles fall in across the horizon in a finite proper time. This sign is also uniquely picked out by models in which the black hole is formed by a collapse process. (The opposite, positive, sign corresponds to a white hole, covering regions I and IV of the Kruskal manifold.) At the horizon we therefore have

$$b_2 = -b_1 \quad \text{at } r = 2M, \quad (15)$$

and combining this with the identity $a_1 b_1 - a_2 b_2 = 1$ we find that

$$a_1 b_2 - a_2 b_1 = -1 \quad \text{at } r = 2M. \quad (16)$$

The diagonal form of the Schwarzschild metric sets $a_1 b_2 - a_2 b_1 = 0$, so does not satisfy Eq. (16) and is not globally admissible. This reflects the fact that the time coordinate is only defined outside the horizon, and the horizon itself is not dealt with correctly.

III. THE DIRAC EQUATION

We now have a general parametrization of the Schwarzschild solution in an arbitrary gauge. The next step is to write down the Dirac equation in this background. This is

$$i g^\mu \nabla_\mu \psi = m\psi, \quad (17)$$

where $g^\mu = e^\mu{}_a \gamma^a$ and

$$\nabla_\mu \psi = \left(\partial_\mu + \frac{i}{2} \Gamma_\mu^{\alpha\beta} \Sigma_{\alpha\beta} \right) \psi, \qquad \Sigma_{\alpha\beta} = \frac{i}{4} [\gamma_\alpha, \gamma_\beta]. \quad (18)$$

The components of the spin connection $\Gamma_\mu^{\alpha\beta}$ are found in the standard way (see Nakahara [12], for example). Rather than setting the γ^a equal to the standard Dirac-Pauli matrices, it is more convenient to reflect the nature of the spherical polar coordinate system and define

$$\begin{aligned} \gamma^t &= \gamma^0, \\ \gamma^r &= \sin\theta(\cos\phi\gamma^1 + \sin\phi\gamma^2) + \cos\theta\gamma^3, \\ \gamma^\theta &= \cos\theta(\cos\phi\gamma^1 + \sin\phi\gamma^2) - \sin\theta\gamma^3, \\ \gamma^\phi &= -\sin\phi\gamma^1 + \cos\phi\gamma^2, \end{aligned} \quad (19)$$

where $\gamma^0, \ldots, \gamma^3$ are the standard (constant) Dirac-Pauli matrices. The reciprocal set has $\gamma_t = \gamma^t$, $\gamma_r = -\gamma^r$, $\gamma_\theta = -\gamma^\theta$, and $\gamma_\phi = -\gamma^\phi$. We will see shortly that working with these polar matrices dramatically simplifies the final form of the Dirac equation. Applying the tetrad of Eq. (4) we now have

$$\begin{aligned} g^t &= a_1 \gamma^0 + a_2 \gamma^r, \qquad g^r = b_1 \gamma^r + b_2 \gamma^0, \\ g^\theta &= \frac{1}{r}\gamma^\theta, \qquad g^\phi = \frac{1}{r\sin\theta}\gamma^\phi \end{aligned} \quad (20)$$

with a reciprocal set of matrices given by

$$\begin{aligned} g_t &= b_1 \gamma_0 - b_2 \gamma_r, \qquad g_r = a_1 \gamma_r - a_2 \gamma_0, \\ g_\theta &= r\gamma_\theta, \qquad g_\phi = r\sin\theta\gamma_\phi. \end{aligned} \quad (21)$$

These matrices satisfy

$$\begin{aligned} \{g^\mu, g^\nu\} = 2g^{\mu\nu} I, \qquad \{g_\mu, g_\nu\} = 2g_{\mu\nu} I, \\ \{g^\mu, g_\nu\} = 2\delta^\mu_\nu I \end{aligned} \quad (22)$$

where μ, ν run over the set (t, r, θ, ϕ), I is the identity matrix, and $g_{\mu\nu}$ is the spacetime metric of Eq. (9). With these choices the spin connection turns out to give

$$g^\mu i\Gamma_\mu^{\alpha\beta}\Sigma_{\alpha\beta} = \left(b_2' + \frac{2b_2}{r} \right)\gamma^0 + \left(b_1' + \frac{2(b_1 - 1)}{r} \right)\gamma^r. \quad (23)$$

Clearly, in order for this expression to be well defined and finite, both b_1 and b_2 must be continuous.

For the Dirac spinor we use a radial separation of the form

$$\psi = \frac{e^{-iEt}}{r}\begin{pmatrix} u_1(r)\chi^{\mu}_{\kappa}(\theta,\phi) \\ u_2(r)\sigma_r\chi^{\mu}_{\kappa}(\theta,\phi)\end{pmatrix} \tag{24}$$

where E is the (complex) energy and

$$\sigma_r = \sin\theta(\cos\phi\sigma_1 + \sin\phi\sigma_2) + \cos\theta\sigma_3. \tag{25}$$

The angular eigenmodes are labeled by κ, which is a positive or negative nonzero integer, and μ, which is the total angular momentum in the $\theta = 0$ direction. Our convention for these eigenmodes is that

$$(\boldsymbol{\sigma}\cdot\boldsymbol{L} + \hbar)\chi^{\mu}_{\kappa} = \kappa\hbar\chi^{\mu}_{\kappa}, \qquad \kappa = \ldots, -2, -1, 1, 2, \ldots. \tag{26}$$

The positive and negative κ modes are related by

$$\sigma_r\chi^{\mu}_{\kappa} = \chi^{\mu}_{-\kappa}. \tag{27}$$

The trial function (24) results in the pair of coupled first-order equations

$$\begin{pmatrix} b_1 & b_2 \\ b_2 & b_1\end{pmatrix}\begin{pmatrix} u_1' \\ u_2'\end{pmatrix} = \boldsymbol{B}\begin{pmatrix} u_1 \\ u_2\end{pmatrix} \tag{28}$$

where

$$\boldsymbol{B} = \begin{pmatrix} \kappa/r - b_1'/2 + ia_2E & i(m + a_1E) - b_2'/2 \\ -i(m - a_1E) - b_2'/2 & -\kappa/r - b_1'/2 + ia_2E\end{pmatrix}. \tag{29}$$

These are the equations we wish to solve for complex energy E. It is first worthwhile confirming that the equations are gauge invariant. A redefinition of the time coordinate is equivalent to the transformations described in Eq. (12). These are combined with the transformation

$$u_1 \mapsto u_1e^{-iE\alpha}, \qquad u_2 \mapsto u_2e^{-iE\alpha} \tag{30}$$

which together ensure that Eq. (28) is still satisfied. The radial boost of the tetrad frame defined by Eq. (13) is combined with the transformation

$$\begin{pmatrix} u_1 \\ u_2\end{pmatrix} \mapsto \begin{pmatrix} \cosh(\beta/2) & -\sinh(\beta/2) \\ -\sinh(\beta/2) & \cosh(\beta/2)\end{pmatrix}\begin{pmatrix} u_1 \\ u_2\end{pmatrix} \tag{31}$$

to again ensure that the equation is still satisfied. In either case we see that the eigenvalue E is unchanged, so it is a true gauge-invariant quantity.

The angular separation of Eq. (24) is clearly justified from the form of the Dirac equation. The separation into energy eigenstates is gauge invariant, but it is helpful to see the separation in a gauge where the Dirac equation takes on a Hamiltonian form. This is provided by the Newtonian gauge of Eq. (8). In this gauge the Dirac equation takes on the simple form [4,11]

$$i\partial\!\!\!/\psi - i\gamma^0\left(\frac{2M}{r}\right)^{1/2}\left(\frac{\partial}{\partial r} + \frac{3}{4r}\right)\psi = m\psi, \tag{32}$$

where $\partial\!\!\!/$ is the Dirac operator in flat Minkowski spacetime. To see this one can introduce standard Cartesian coordinates

$$x = r\sin\theta\cos\phi, \qquad y = r\sin\theta\sin\phi, \qquad z = r\cos\theta. \tag{33}$$

We then find that

$$\gamma^0\partial_t + \gamma^r\partial_r + \frac{1}{r}\gamma^{\theta}\partial_{\theta} + \frac{1}{r\sin\theta}\gamma^{\phi}\partial_{\phi} = \gamma^0\partial_t + \gamma^1\partial_x + \gamma^2\partial_y + \gamma^3\partial_z = \partial\!\!\!/, \tag{34}$$

which is the reason behind our choice of matrices in Eq. (19). Equation (32) is manifestly separable in time, so it has solutions that go as $\exp(-iEt)$. Since the separation works in this gauge, it must work in all others. We will return to this gauge choice when we turn to finding the energy spectrum.

The nature of Eq. (28) can be understood more clearly by writing it in the form

$$(1 - 2M/r)\begin{pmatrix} u_1' \\ u_2'\end{pmatrix} = \begin{pmatrix} b_1 & -b_2 \\ -b_2 & b_1\end{pmatrix}\boldsymbol{B}\begin{pmatrix} u_1 \\ u_2\end{pmatrix}. \tag{35}$$

This exposes the fact that the horizon is a regular singular point of the radial equations. The same is true of the origin. But infinity turns out to be an irregular singular point. Taken together, these imply that the radial equations cannot be manipulated into a second-order hypergeometric form, as one is able to do for the hydrogen atom. The closest the equations come to a recognizable form is that of Heun's equation, which generalizes the hypergeometric equation to the case of four regular singular points on the complex plane [13]. But Heun's equation can usually only be analyzed using numerical techniques, and these are the tools we will apply to Eq. (28).

The presence of singular points means that we must check carefully that our solutions behave appropriately at these points. The point at infinity is not an issue, as we seek solutions that decay exponentially. Similarly, the origin is not a problem. We expect that the function will be weakly singular there as the origin acts as a current sink, and this is indeed the case. The horizon, however, is more complicated. The wave function must be well behaved at the horizon if it is to represent a physical solution. To test this we introduce the series expansion

$$u_1 = \eta^s\sum_{k=0}^{\infty}\alpha_k\eta^k, \qquad u_2 = \eta^s\sum_{k=0}^{\infty}\beta_k\eta^k, \tag{36}$$

where $\eta = r - 2M$. On substituting this series into Eq. (35), and setting $\eta = 0$, we obtain the indicial equation

$$\det\left[\begin{pmatrix} b_1 & -b_2 \\ -b_2 & b_1\end{pmatrix}\boldsymbol{B} - \frac{s}{r}I\right]_{r=2M} = 0, \tag{37}$$

where I is the identity matrix. Employing the result that

$$b_1 b_1' - b_2 b_2' = M/r^2 \tag{38}$$

we find that the two solutions of the indicial equation are

$$s = 0, -\tfrac{1}{2} + 4iME(b_1 a_2 - b_2 a_1)_{r=2M}. \tag{39}$$

Equation (16) then tells us that the two indices are

$$s = 0, -\tfrac{1}{2} + 4iME. \tag{40}$$

These indices are therefore gauge invariant. The regular root $s = 0$ ensures that we can always construct a solution that is finite and continuous at the horizon. The singular branch gives rise to discontinuous solutions with an outgoing current at the horizon. These can be used to provide a heuristic explanation of the Hawking radiation [11]. It is clear that the nonzero indicial root gives rise to a wave function that is ill defined at the horizon, and so cannot represent a physical state. We must therefore confine our search for bound states to solutions that are regular at the horizon.

The regular and singular solutions are related by a generalized form of time-reversal symmetry. For this we define

$$\bar{\psi}(t, \boldsymbol{x}) = \frac{1}{(1 - 2M/r)^{1/2}} (b_1 \gamma_0 - b_2 \gamma_r) \psi^*(-t + f(r), \boldsymbol{x}), \tag{41}$$

which effectively reverses the time direction using the normalized timelike Killing vector. In terms of the u_1 and u_2 functions, the new solution is characterized by

$$\begin{pmatrix} \bar{u}_1 \\ \bar{u}_2 \end{pmatrix} = \frac{\exp(-iE^* f(r))}{(1 - 2M/r)^{1/2}} \begin{pmatrix} b_1 & b_2 \\ -b_2 & -b_1 \end{pmatrix} \begin{pmatrix} u_1^* \\ u_2^* \end{pmatrix}, \tag{42}$$

where $f(r)$ is determined by

$$(1 - 2M/r) \partial_r f(r) = 2(a_1 b_2 - a_2 b_1). \tag{43}$$

The time-reversed solution has energy E^* and so is exponentially growing in time. It is singular at the horizon, and is not normalizable.

Eigenmodes with different values of κ and μ are orthogonal. For states with the same values of κ and μ the quantum inner product can be taken as

$$\langle \psi \mid \phi \rangle = \int_0^\infty dr (a_1 (u_1^* v_1 + u_2^* v_2) + a_2 (u_2^* v_1 + u_1^* v_2)), \tag{44}$$

where the u_i and v_i denote the radial functions in ψ and ϕ respectively. Current conservation for the Dirac equation is summarized in the relation

$$\begin{aligned} &\frac{\partial}{\partial t} (a_1 (u_1 u_1^* + u_2 u_2^*) + a_2 (u_1 u_2^* + u_2 u_1^*) e^{-i(E - E^*)t}) \\ &\quad = -\frac{\partial}{\partial r} (b_1 (u_1 u_2^* + u_2 u_1^*) + b_2 (u_1 u_1^* + u_2 u_2^*) e^{-i(E - E^*)t}). \end{aligned} \tag{45}$$

Again it is straightforward to confirm that this equation is gauge invariant. The right-hand side of this equation defines r^2 times the radial flux. We denote this by F,

$$F(r) = b_1 (u_1 u_2^* + u_2 u_1^*) + b_2 (u_1 u_1^* + u_2 u_2^*). \tag{46}$$

For spatially normalizable states we must have $F \mapsto 0$ as $r \mapsto \infty$. But at the horizon we also have

$$F = -b_1 |u_1 - u_2|^2, \tag{47}$$

which defines an inward-pointing current. At the horizon, the regular solution has

$$|u_1 - u_2|^2 = |\alpha_0 - \beta_0|^2, \tag{48}$$

using the power series expansion of Eq. (36). The coefficients are related by

$$\begin{aligned} &\left(iE - \frac{1}{8M} + b_1 \left(\frac{\kappa}{2M} - im \right) \right) \alpha_0 \\ &\quad = \left(-iE + \frac{1}{8M} + b_1 \left(\frac{\kappa}{2M} - im \right) \right) \beta_0. \end{aligned} \tag{49}$$

It is therefore impossible to satisfy $\alpha_0 = \beta_0$ for finite energy, so there must be a nonvanishing inward current present at the horizon [14]. This in turn tells us that the state must decay. This decay takes place at the origin, where unitary evolution breaks down [11,15]. For bound states the energy E must contain real and imaginary terms, so we set

$$E = \omega - i\nu. \tag{50}$$

Current conservation now takes the form

$$\frac{dF}{dr} = 2\nu (a_1 (u_1 u_1^* + u_2 u_2^*) + a_2 (u_1 u_2^* + u_2 u_1^*)). \tag{51}$$

Given a set (u_1, u_2, E, κ) that solves the radial equation (28) a new solution set is generated by the transformation

$$(u_1, u_2, E, \kappa) \mapsto (u_2^*, u_1^*, -E^*, -\kappa). \tag{52}$$

It follows that the real part of the energy spectrum is symmetric about the zero point. That is, for a state with real energy ω a corresponding antiparticle state exists with real energy $-\omega$. The decay rate is the same for both states, however. If we assume that the vacuum is constructed from the Dirac sea of negative energy states, then this vacuum will decay in time. A loss of negative energy states can be equally interpreted as the generation of positive energy states, which provides a suggestive physical model for Hawking radiation.

IV. THE ENERGY SPECTRUM

To solve for the energy spectrum we work mainly in the Newtonian gauge of Eq. (8). In this gauge the interaction with the black hole is defined solely by an interaction Hamiltonian $H_{\rm I}$ given by

$$H_{\rm I}\psi = i\hbar\left(\frac{2GM}{r}\right)^{1/2}\frac{1}{r^{3/4}}\frac{\partial}{\partial r}(r^{3/4}\psi). \tag{53}$$

Dimensional constants are included in a number of equations in this section to illustrate certain features of the problem. The line element for the Newtonian gauge has flat spatial sections for constant t, so the quantum inner product between states has the simple flat-space form

$$\langle\psi \mid \phi\rangle = \int dxdydz\psi^\dagger\phi \tag{54}$$

where x, y, z are the Cartesian coordinates of Eq. (33) and all integrals run from $-\infty\cdots\infty$. The interaction Hamiltonian is not Hermitian, as we have

$$H_{\rm I} - H_{\rm I}^\dagger = -i\hbar(2GMr^3)^{1/2}\delta(x)\delta(y)\delta(z). \tag{55}$$

It is straightforward to check that all wave functions approach the origin as $r^{-3/4}$, so the non-Hermitian part of $H_{\rm I}$ has finite expectation. This confirms that Hermiticity only breaks down at the origin, as stated earlier. In this respect it may be more natural to refer to $H_{\rm I}$ as a ''pseudo-Hamiltonian,'' in the sense of an operator acting on an open quantum system [16]. There is no doubt that the system described here is open, as the singularity is not treated as part of the quantum system. But the system is only open in an extremely simple fashion. There is no ambiguity in either the time evolution of the state, or the correct definition of the observable energy. Time evolution is defined by the Dirac equation, in whichever gauge one chooses to adopt, and the energy is defined by the energy-momentum tensor. The fact that we have a Hamiltonian description at all is a result of a series of gauge choices, so one must be careful not to place too strong an interpretation on the gauge-dependent quantity $H_{\rm I}$.

The bound state energy eigenspectrum is determined entirely by the properties of the wave function at the horizon and at infinity. The demands that the wave function is finite at the horizon and falls off exponentially at infinity are sufficient to produce the spectrum. But it is only by considering the global properties of the wave function that the imaginary contribution to the energy is fully understood. Decay only takes place at the singularity, and the decay rate for a given eigenstate is naturally related to the behavior of the wave function near the singularity. If the spatial degrees of freedom in an energy eigenstate are normalized such that

$$\int_0^\infty dr(u_1u_1^* + u_2u_2^*) = 1 \tag{56}$$

then the imaginary component of the energy, $-i\nu$, is determined by

$$\nu = \lim_{r\mapsto 0}\frac{\hbar(2GM)^{1/2}}{2}\frac{1}{r^{3/2}}(u_1u_1^* + u_2u_2^*). \tag{57}$$

This identity only holds if the state is globally normalized. It provides a further independent check that the solutions we obtain numerically are globally normalizable bound states. The decay rate increases for states with a larger probability density near the singularity, as one would expect. The fact that the states approach the origin as $r^{-3/4}$ ensures that the radial probability density tends smoothly to zero at the singularity. The presence of the singularity does not prevent the formation of normalizable states, and the singular nature of the wave function is no worse than that of the ground state of the hydrogen atom.

The interaction Hamiltonian is independent of the speed of light, so the nonrelativistic approximation to the Dirac equation results in the Schrödinger equation

$$-\frac{\hbar^2\boldsymbol{\nabla}^2}{2m}\psi_{\rm NR} + i\hbar\left(\frac{2GM}{r}\right)^{1/2}\frac{1}{r^{3/4}}\frac{\partial}{\partial r}(r^{3/4}\psi_{\rm NR}) = E_{\rm NR}\psi_{\rm NR}, \tag{58}$$

where the subscript NR denotes nonrelativistic. If we now introduce the phase-transformed variable

$$\Psi = \psi_{\rm NR}\exp(-i(8r/a_0)^{1/2}) \tag{59}$$

where

$$a_0 = \frac{\hbar^2}{GMm^2} \tag{60}$$

we see that Ψ satisfies

$$-\frac{\hbar^2\boldsymbol{\nabla}^2}{2m}\Psi - \frac{GMm}{r}\Psi = E_{\rm NR}\Psi. \tag{61}$$

In the nonrelativistic limit the energy spectrum is therefore given by the gravitational analog of the hydrogen atom spectrum [9],

$$E_{\rm NR} = -\frac{G^2M^2m^3}{2\hbar^2}\frac{1}{n^2}, \qquad n = 1, 2, \ldots. \tag{62}$$

In terms of the Planck mass m_p we can also write

$$E_{\rm NR} = -\left(\frac{Mm}{m_p^2}\right)^2\frac{mc^2}{2n^2}. \tag{63}$$

The fact that we have a reasonable starting point for the spectrum in the weak-coupling limit is valuable, as our method involves searching for eigenvalues over the complex energy plane. By analogy with the hydrogen atom case, we expect that the nonrelativistic spectrum will be a reasonable approximation provided

$$\frac{Mm}{m_p^2} \ll 1. \tag{64}$$

Returning to the full, relativistic equation (28), we convert this to dimensionless form by introducing the dimensionless distance variable

$$x = \frac{rc^2}{GM}, \tag{65}$$

which ensures that the horizon lies at $x = 2$. We also introduce the dimensionless coupling coefficient

$$\alpha = \frac{Mm}{m_p^2} \tag{66}$$

and energy

$$\varepsilon = \frac{EM}{c^2 m_p^2}. \tag{67}$$

In terms of these our eigenvalue problem becomes

$$(x-2)\begin{pmatrix} u_1' \\ u_2' \end{pmatrix} = \begin{pmatrix} 1 & (2/x)^{1/2} \\ (2/x)^{1/2} & 1 \end{pmatrix} \begin{pmatrix} \kappa & ix(\alpha+\varepsilon) - (8x)^{-1/2} \\ -ix(\alpha-\varepsilon) - (8x)^{-1/2} & -\kappa \end{pmatrix} \begin{pmatrix} u_1 \\ u_2 \end{pmatrix} \tag{68}$$

where the primes now denote derivatives with respect to x. We seek eigenvalues ε for fixed coupling α.

Two complementary methods are employed to solve the eigenvalue problem. We start with a series expansion around the horizon of the regular branch of the solution. The restriction to this branch removes 2 degrees of freedom at the horizon, so the function is uniquely specified up to an overall magnitude and phase. These are chosen conveniently by setting $u_1 = 1$ at the horizon. The power series expansion extends the solution a short distance away from the horizon, from where the values of (u_1, u_2) can be used to initiate numerical integration of the differential equation (68). For most values of ε the numerical integrator will start to increase exponentially after a finite distance. The aim initially is to vary ε so as to push this distance out as far as possible. This requires a reasonable initial guess for the eigenvalues, which is where the nonrelativistic approximation is helpful to get things started.

Once we have achieved a reasonably accurate value for ε, we turn to a more sophisticated method to improve accuracy. We seek normalizable states for which ψ is finite over all space. To be confident we have found such a state we need to numerically integrate inwards from infinity, as well as outwards from the horizon. If the solutions for u_1 and u_2 can be arranged to match at some suitable radius then we have found a global solution to the first-order equation (68). To expand about infinity we need to take care of the essential singularity present there. A suitable series expansion is provided by

$$\begin{pmatrix} u_1 \\ u_2 \end{pmatrix} = \exp\left(-px + 2i\varepsilon(2x)^{1/2} + \frac{\alpha^2 - 2p^2}{p}\ln x\right) \times \sum_{n=0} \begin{pmatrix} \alpha_{n/2} x^{-n/2} \\ \beta_{n/2} x^{-n/2} \end{pmatrix} \tag{69}$$

where

$$p^2 = \alpha^2 - \varepsilon^2 = \frac{M^2}{m_p^4 c^4}(m^2c^4 - E^2). \tag{70}$$

The definition of p involves a complex square root, and the branch is chosen so that p has a positive real value, ensuring the wave function falls off exponentially.

The fact that only one root of the indicial equation is used implies that, for a given ε, ψ is specified at infinity up to an arbitrary magnitude and phase. The first few terms in the series expansion (69) are used to compute ψ at a finite radius and these values are then numerically integrated inwards. A certain amount of fine-tuning is then required to pick the radius at which to attempt matching. Once a radius is chosen the matching condition is that the inward and outward values of the two complex functions u_1 and u_2 agree. This condition is converted into a set of four scalar equations which state that the real and imaginary differences vanish. In addition we have four arbitrary parameters to vary—the real and imaginary terms in the energy, and the magnitude and phase of the function integrated inwards from infinity. This system of four equations and four unknowns is then solved by a Newton-Raphson method. This converges very quickly and affords good control over accuracy.

A number of independent checks were performed on the energy spectrum achieved by this method. The first was that the calculations were repeated using the same scheme in a different gauge. The gauge chosen for comparison was that defined by advanced Eddington-Finkelstein coordinates, using the form of Eq. (7). The second test involved using a minimax routine to find the energy spectrum. This method is less accurate, but gave good agreement for the states of lowest energy [17]. A further check was to confirm that in the limit as $M \mapsto 0$ the spectrum and states approach that of the Dirac hydrogen atom, as expected from the nonrelativistic limit. The final check was to confirm that, after normalization, the states satisfy the identity of Eq. (57). This check was again satisfied to high precision.

V. RESULTS

The real parts of the energy for the three lowest-energy states are plotted in Fig. 1. The vertical axis plots the real part of the energy in units of the rest energy of the particle, which is given by

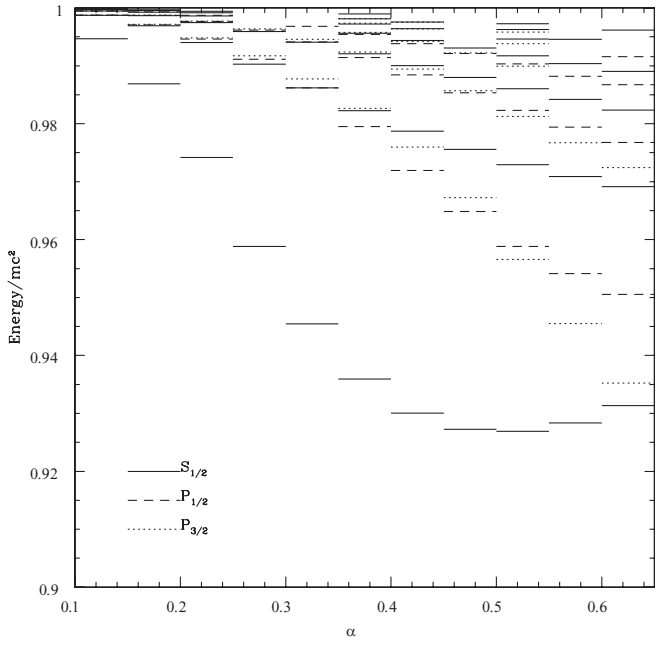

FIG. 1. The real part of the bound state energy, in units of mc^2. The horizontal axis labels the dimensionless coupling coefficient α, and the lines represent the value of the energy for the coupling at the left of the line, with α ranging from 0.1 to 0.6 in steps of 0.05. The $S_{1/2}$, $P_{1/2}$ and $P_{3/2}$ orbits are shown.

$$\frac{E}{mc^2} = \frac{\varepsilon}{\alpha}. \tag{71}$$

The fact that we obtain this dimensionless ratio reflects the equivalence principle. The mass m does not effect the spectrum on its own—the spectrum only depends on the product mM. States are labeled using the standard spectroscopic scheme. In this scheme $\kappa = 1$ corresponds to $S_{1/2}$, $\kappa = 2$ to $P_{3/2}$ and $\kappa = -1$ to $P_{1/2}$. For each eigenvalue κ a ladder of levels is obtained.

The energy spectrum illustrates a number of remarkable features. For small α the spectrum resembles that of a hydrogen atom. But as the coupling increases the energy of the $1S_{1/2}$ state reaches a minimum and then starts to increase. The gravitational case avoids the $Z = 137$ catastrophe of the relativistic Coulomb problem. This is to be expected—coupling strengths with $\alpha > 1$ are routinely achieved astrophysically and such objects appear to be stable. We also see that as α increases beyond 0.6 the $P_{3/2}$ state appears to take over as the ground state. This is confirmed in Fig. 2, which shows the spectra of the $S_{1/2}$, $P_{3/2}$ and $D_{5/2}$ states out to $\alpha = 1.4$. We see clearly that around $\alpha = 0.6$ the $2P_{3/2}$ state takes over from $1S_{1/2}$ as the ground state, only to be replaced in turn by the $3D_{5/2}$ state at $\alpha = 1.2$. An explanation of this phenomena can be found in the classical expression for the binding energy in a Schwarzschild potential.

For a particle of mass m in a Schwarzschild background the dynamics reduces to motion in the effective radial potential

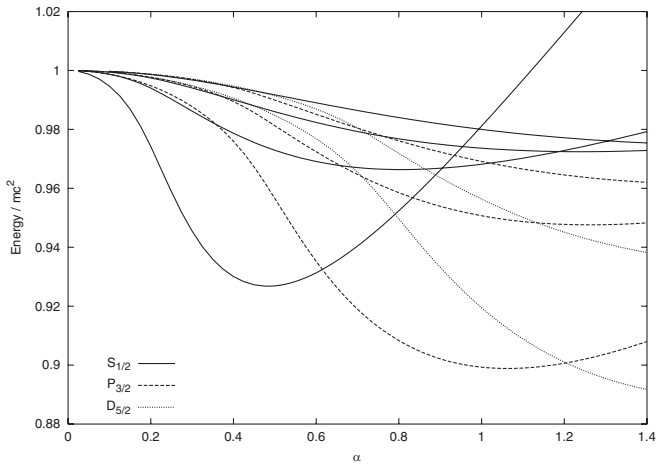

FIG. 2. The energy spectra of the $S_{1/2}$, $P_{3/2}$ and $D_{5/2}$ states. At around $\alpha = 0.6$, the $2P$ state becomes the ground state, and beyond $\alpha = 1.2$ it is replaced by the $3D$ state.

$$V_{\text{eff}} = -\frac{GMm}{r} + \frac{J^2}{2mr^2}\left(1 - \frac{2GM}{c^2 r}\right), \tag{72}$$

where J is the angular momentum of the particle. This is illustrated in Fig. 3. For $J > \sqrt{12}GMm/c$, classical bound states can exist as the effective potential has a minimum, but if the particle's angular momentum is smaller than $\sqrt{12}GMm/c$ it becomes insufficient to support a classical orbit. For a circular orbit at radius r the conserved relativistic energy, conjugate to time translation, is

$$E = mc^2 \frac{r - 2GM/c^2}{r^{1/2}(r - 3GM/c^2)^{1/2}}. \tag{73}$$

The radius r and angular momentum J are related by

$$\frac{J^2}{m^2} = \frac{GMr^2}{r - 3GM/c^2}. \tag{74}$$

Now suppose we attempt a form of naive Bohr quantization by setting

$$J = n\hbar. \tag{75}$$

Converting to dimensionless quantities the effective potential becomes

$$\frac{V_{\text{eff}}}{mc^2} = -\frac{1}{x} + \frac{n^2}{2\alpha^2 x^2}\left(1 - \frac{2}{x}\right), \tag{76}$$

and the orbital energy is

$$\frac{\varepsilon}{\alpha} = \frac{x - 2}{(x(x-3))^{1/2}} \tag{77}$$

where

$$x = \frac{n^2}{2\alpha^2}\left(1 + \left(1 - \frac{12\alpha^2}{n^2}\right)^{1/2}\right). \tag{78}$$

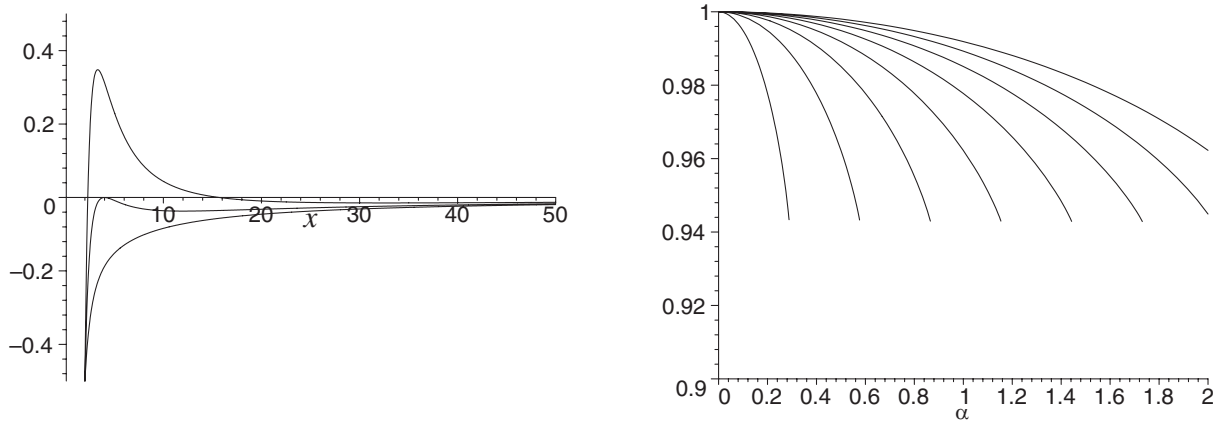

FIG. 3. Bohr quantization of classical circular orbits. The left-hand plot shows the effective potential in units of mc^2 for $\alpha = 0.5$ and $J = n\hbar$, with $n = 1, 2, 3$. For $n = 1$ no classical bound state is possible. As n is increased a minimum forms in the potential, and the barrier between the minimum and the singularity grows larger. The right-hand plot shows the relativistic energy in units of mc^2 as a function of α. The first eight n values are shown. For each n value the minimum energy is achieved when $\alpha = n/\sqrt{12}$.

In the small α regime this reproduces the spectrum of Eq. (63). But as α increases the energy falls to a minimum at $\alpha^2 = n^2/12$, beyond which the orbit no longer exists for a given n (see Fig. 3). The minimum energy achieved is $0.94mc^2$, corresponding to $x = 6$. Inside this radius no stable classical circular orbits exist. In the quantum description we find that as α increases the orbits get more tightly bound around the horizon. As the coupling increases the orbits are dominated by terms inside $x = 6$ and so become energetically less favorable. The ground state is then one of higher angular momentum, for which the orbit is less tightly bound. Figure 2 also shows that as α increases the $1S_{1/2}$ state becomes unbound. This effect is also seen classically, as circular orbits with $r < 4M$ are known to be unbound, as well as unstable.

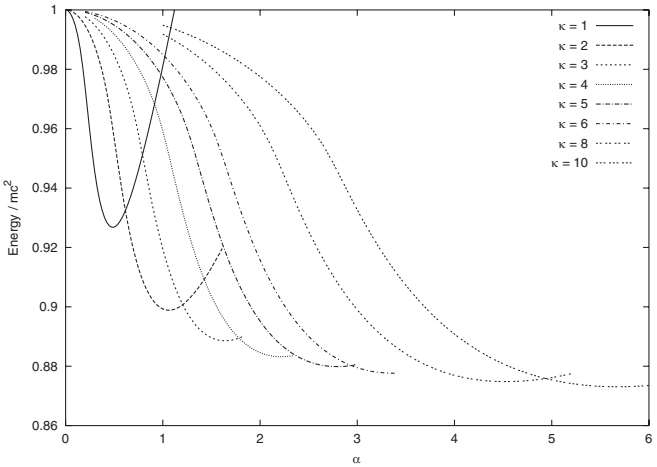

FIG. 4. Energy levels of states with higher angular momenta. This plot shows the energy levels of the lowest-energy states with a range of angular momenta $\kappa = 1 \cdots 10$. It illustrates how each state takes a turn as the ground state, as the coupling is increased. The positions of the energy minima are linearly spaced in α and have increasingly large binding energies.

The form of the effective potential illustrates a further feature of the quantum states, which is that the quantum decay can be interpreted as a tunneling phenomena. This is certainly a valid picture for states with $n > \sqrt{12}\alpha$. For a fixed n, as α increases, the potential barrier decreases and we expect that the tunneling rate onto the singularity will increase. This is indeed the case, as we discuss further in Sec. VII.

Figure 4 shows how states of successively higher angular momentum take over as the ground state as the coupling is increased. In the small α/κ limit, the energy levels resemble those of the classical orbits. At larger couplings, the energy of a given state falls to a minimum, and then begins to increase again, apparently without limit. The α value at which the minimum occurs is roughly proportional to the angular momentum of the state, with $\alpha = 0.58\kappa - 0.10$ providing a good fit. The maximum binding energy available increases with angular momentum, to beyond $E = 0.88mc^2$. This means that quantum mechanics predicts around twice the classical value for the radiation efficiency of accretion processes. To confirm this effect we need to find the limiting value of the binding energy for astrophysical values of α. For an electron around a solar-mass black hole, for example, we have $\alpha = 4 \times 10^{15}$, so a large α limit of our equations should be very accurate.

VI. WAVE FUNCTION PROPERTIES

With our current choice of gauge the radial form of the wave function is best visualized by plotting r^2 times the timelike component of the current. We denote this ρ, so

$$\rho = |u_1|^2 + |u_2|^2. \tag{79}$$

The gauge-invariant definition of ρ is that it is r^2 times the density as measured by observers in radial free fall from

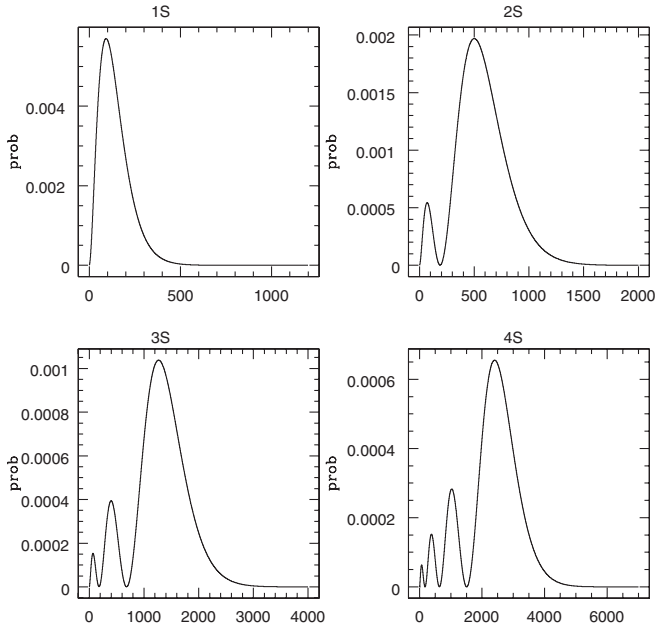

FIG. 5. The radial probability density for the $1S_{1/2}$, $2S_{1/2}$, $3S_{1/2}$ and $4S_{1/2}$ states for a coupling of $\alpha = 0.1$. The horizontal axis is the dimensionless radius x, and the horizon lies at $x = 2$. All plots are started from the horizon. The part of the density inside the horizon is not plotted, though in all cases this smoothly approaches the origin.

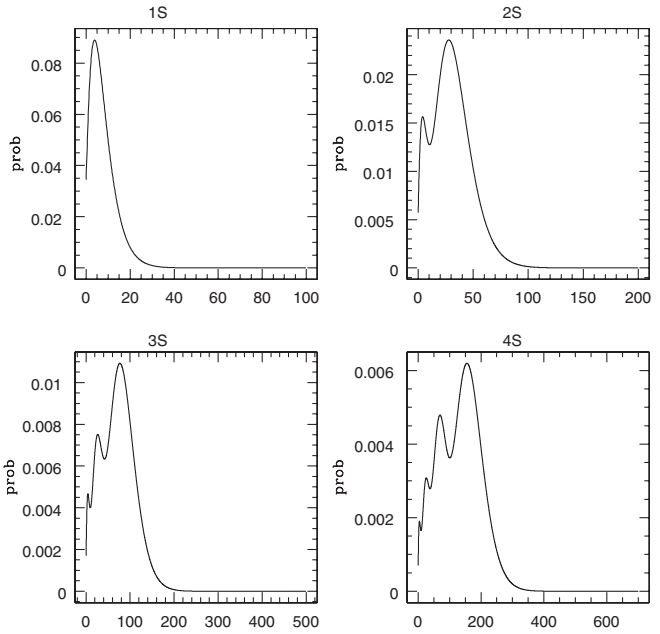

FIG. 6. The radial probability density for the $1S_{1/2}$, $2S_{1/2}$, $3S_{1/2}$ and $4S_{1/2}$ states for a coupling of $\alpha = 0.35$. The nodal pattern seen in Fig. 5 is beginning to get washed out as the wave function compresses around the horizon.

rest at infinity. The first four $S_{1/2}$ states for a small coupling are shown in Fig. 5. The plots are very similar to those for the nonrelativistic hydrogen atom. In all cases the peak of the wave function is a long way outside the horizon, with only a small fraction of the probability density lying inside the horizon.

As we increase the coupling to $\alpha = 0.35$ we obtain the series of plots in Fig. 6. Predictably, the wave functions start to bunch in closer to the horizon. Slightly more surprisingly, the nodal structure disappears for larger couplings. The density no longer drops down to near zero at a number of nodes, but instead a number of dips are present. If we increase the coupling further still, to $\alpha = 0.5$, the dips themselves are largely washed out and we obtain the somewhat structureless plots shown in Fig. 7.

Some additional insight into the nature of the orbitals is obtained by calculating the expectation value of r. With our current gauge choices this is defined in the obvious manner as

$$\langle r \rangle = \frac{\int_0^\infty dr r(|u_1|^2 + |u_2|^2)}{\int_0^\infty dr(|u_1|^2 + |u_2|^2)}. \tag{80}$$

These are calculated via a straightforward Simpson's rule, and the results for the S, P and D orbitals are shown in Fig. 8. We see that $\langle r \rangle$ decreases as the coupling increases. In the low-alpha regime, the expectation value follows the radius of the classical circular orbit, so $\langle r \rangle \propto \alpha^{-2}$. As the coupling increases, and stable orbits become classically impossible, we find that $\langle r \rangle$ approaches, and moves within, the horizon. For higher α the bulk of the probability density lies inside the horizon, representing a short-lived state of a tightly bound particle.

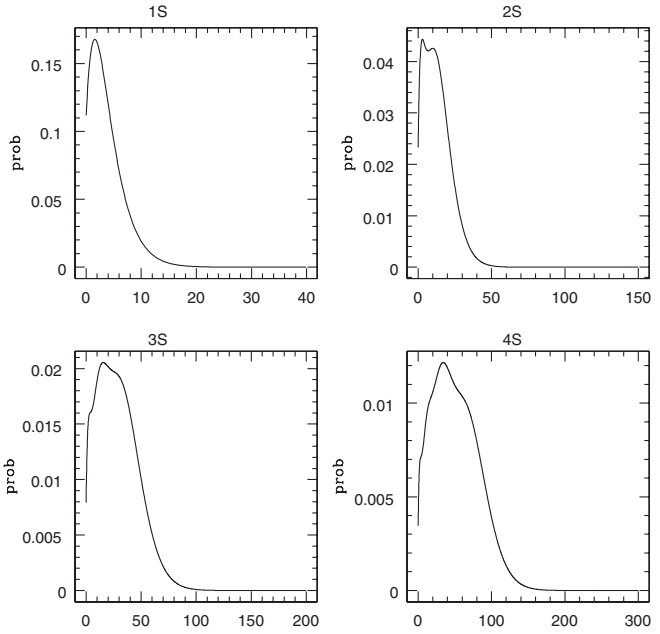

FIG. 7. The radial probability density for the $1S_{1/2}$, $2S_{1/2}$, $3S_{1/2}$ and $4S_{1/2}$ states for a coupling of $\alpha = 0.5$. The pattern of nodes and dips seen in Figs. 5 and 6 has almost completely vanished, leaving a series of density profiles that lack structure.

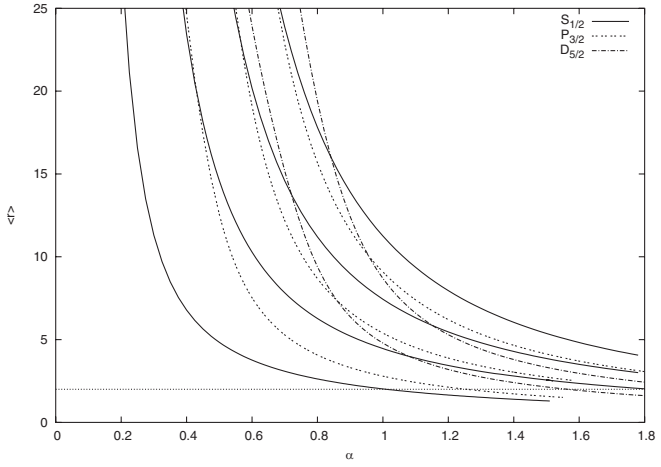

FIG. 8. The expectation value of r in units of GM/c^2 for the S, P and D states. The broken horizontal line at $x = 2$ shows the position of the horizon.

While the low angular momentum orbitals are concentrated near the horizon, the orbitals with larger angular momentum still lie an appreciable distance out. As such, they adopt a form closer to the familiar hydrogen atom orbitals. A series of such orbitals is shown in Fig. 9, which shows the first-excited mode for κ values of 1, 2, 3 and 4. The coupling is again set to 0.5. As expected, the probability density is concentrated successively further from the hole. By the time we reach $\kappa = 3$ (a classical radius of $x =$ 33) the wave function returns to the familiar hydrogenlike form.

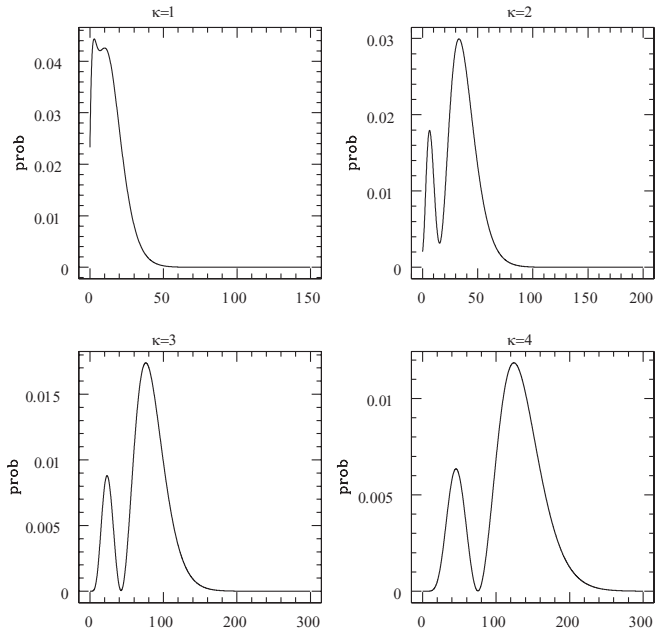

FIG. 9. The radial probability density for a range of angular momentum values with a coupling of $\alpha = 0.5$. The first-excited states are shown for $\kappa = 1, 2, 3, 4$. As κ increases the orbitals are concentrated further from the source, and begin to resemble hydrogen atom wave functions.

VII. DECAY RATES

So far we have concentrated on the real part of the energy, and the associated orbitals. But the fact that the black hole effective Hamiltonian is not Hermitian implies that the energy is not real and the states have a finite half-life. As such the solutions could be viewed as representing resonance states as opposed to bound states. But for suitably large angular momenta the half-lives can be pushed up as high as desired and the states will be extremely long lived. Such states are appropriate for a quantum description of a particle in a classically stable orbit some distance from the horizon.

As argued above, the imaginary part of the energy will be negative, corresponding to a decay. The behavior of this decay can be visualized in a number of ways. With $E = \omega - i\nu$, the relevant quantity to study is

$$a = \frac{\nu}{mc^2}. \tag{81}$$

In Fig. 10 we plot a as a function of coupling for the $1S_{1/2}$ state. For comparison the real part of the energy is also plotted. The real energy falls to a minimum and starts increasing again as the orbits become unfavorably close, whereas the imaginary term simply increases monotonically. This is as one would expect, as Fig. 8 showed that the orbits become increasingly tightly bound as α increases. As the coupling strength reaches 1, the imaginary component of the energy is of the order of 0.3 times the rest energy of the particle. This implies that the orbit should decay on the time scale defined by the Compton frequency. These states are therefore extremely short lived, with a resonance width comparable to the orbital energy.

In Fig. 11 a is plotted for states with a range of angular momenta, $\kappa = 1 \cdots 5$. The set of lowest-energy states ($1S_{1/2}$, $2P_{3/2}$, ...) is compared to the set of first-excited states ($2S_{1/2}$, $3P_{3/2}$, ...). Both plots show the expected monotonic increase in a with coupling strength as the orbits become more tightly bound and a greater percentage of the wave function lies inside the horizon. The first-excited states are less tightly bound than the ground states, so have smaller decay rates. Below a threshold value of α, the imaginary energy is negligible. This threshold depends roughly linearly on κ, and is the same for the lowest and first-excited states. Using the effective-potential model, we would expect decay to become dominant beyond the last value of α that allows stable circular orbits, $\alpha = \kappa/\sqrt{12} = 0.29\kappa$. The plot suggests that this model is reasonably valid. States with higher angular momentum can therefore be extremely stable, as the increase in κ keeps the bulk of density away from the singularity.

A classical argument can also be used to relate the high-α behavior of the imaginary energy to the expectation

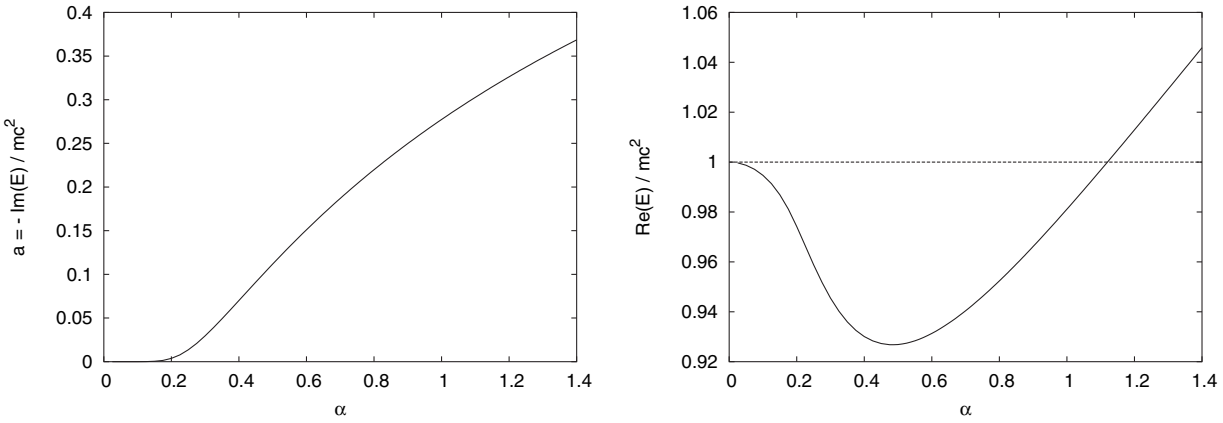

FIG. 10. The imaginary and real energies for the $1S_{1/2}$ state. The left-hand plot shows (minus) the imaginary component of the energy as a function of the coupling strength. As expected, this increases as the orbits become more tightly bound. For comparison, the more complicated behavior of the real part of the energy is shown on the right-hand side.

value of wave function radius, by considering the proper time for radial infall. A massive particle starting at radius r_i from rest would take proper time

$$\tau_{\text{infall}} = \sqrt{\frac{r_i^3}{8GM}}\pi \tag{82}$$

to reach the singularity. Conversely, the typical decay time for the wave function is

$$\tau_{\text{decay}} = \frac{\hbar}{amc^2}. \tag{83}$$

If the decay time is similar to the infall time from the wave function expectation position $\langle x\rangle$, we would expect

$$a\alpha \propto \langle x\rangle^{-3/2}. \tag{84}$$

This model works well for the $1S_{1/2}$ state, and we find $a\alpha \propto \langle x\rangle^{-1.6}$ in the high-α regime. The model requires some modifications for states with orbital angular momentum, as the infall time takes a more complicated form.

With the decay rates now obtained, we can return to Eq. (57) to check the consistency of our method. For a number of states we computed the normalization integral and also extracted the behavior of the state near the singularity. For all of these the imaginary component of the energy was consistent with Eq. (57). This confirms that the states are normalizable and represent genuine bound states.

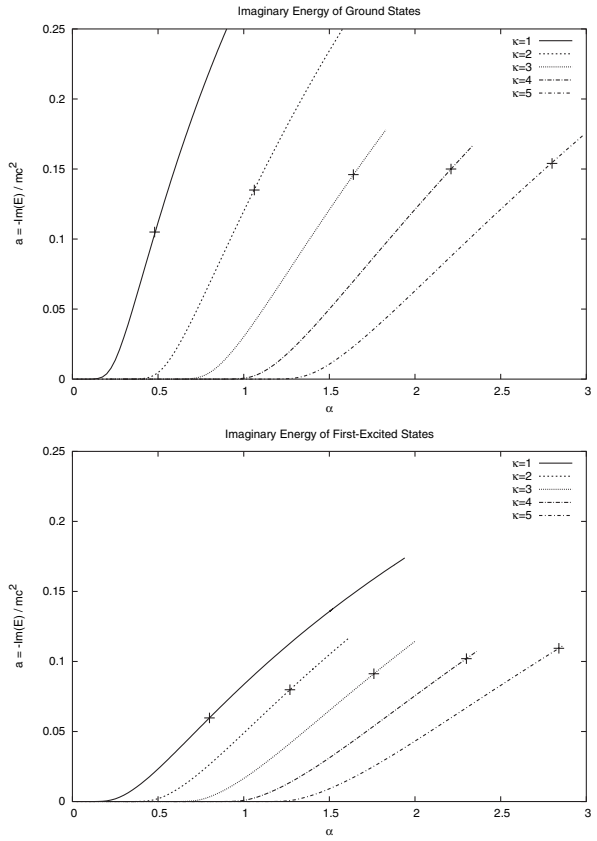

FIG. 11. The imaginary energies of states with a range of angular momenta $\kappa = 1 \cdots 5$. The top plot shows the decay rates of the ground states, and the bottom plot shows the decay rates of the first-excited states, as functions of the coupling strength α. The positions of the minima in the real energy are marked with crosses.

VIII. DISCUSSION

We have demonstrated the existence of a complicated spectrum of bound states for a quantum fermion in a black hole background. Each state represents a spatially normalizable solution to the Dirac equation in a Schwarzschild background. The fact that time-separable solutions exist is simply established in one particular gauge, which casts the equation in a Hamiltonian-like form. A study of the behavior of the wave function under gauge transformations shows that time separability is a gauge-invariant feature. The spectrum itself is determined by boundary conditions applied at the horizon and at infinity. These alone are sufficient to imply the existence of an imaginary (decay)

contribution to the energy. The physical explanation for this is provided by the singularity, which acts as a current sink.

The qualitative features of the spectrum can be understood in terms of simple semiclassical models, but a full quantitative understanding only seems possible through a mixture of computational methods. The work in this paper can clearly be extended in a number of ways. We have only plotted the spectrum at low coupling strengths of $\alpha \sim 1$, but astrophysical values can be far larger than this, with $\alpha \sim 10^{15}$ for solar-mass black holes. For larger α, the ground state will be one of high angular momentum. In this regime the spectrum will be quite different to that of the hydrogen atom. One important question is precisely how great a binding energy can be achieved. In Fig. 4 we see that at around $\alpha = 5$ we are achieving total energies of $0.88mc^2$, which is significantly lower than the classical value of $0.94mc^2$. This suggests that more energy may be available in accretion processes than is traditionally thought.

As well as increasing α, it would be of considerable interest to repeat this work for the case of a Kerr black hole. In this respect a useful start has been made in [18], where the Kerr solution is written in a form that generalizes the Newtonian gauge employed in this paper. The calculations for the Kerr case are more complicated, however, because the angular separation constants are energy dependent [2,9]. There are also signs that the horizon structure of the Kerr solution will complicate the fairly straightforward picture presented here. The problem can be seen by analyzing the behavior in a Reissner-Nordstrom background using the setup of this paper. For this case we find that the regular solutions at the outer horizon do not match regular solutions at the inner horizon. So quantum mechanics predicts that the probability density will pile up around the inner horizon in a similar manner to the classical picture. Behavior of this type is inevitable, as the Reissner-Nordstrom singularity does not act as a sink, and the Hamiltonian is Hermitian. Since the current must still be inward pointing at the outer horizon, the probability density has to pile up somewhere. It seems likely that a similar picture holds for the Kerr solution, but detailed calculations are required to confirm this.

The energy spectra presented in this paper raise a number of fundamental issues, which demonstrate the limitations in our current understanding of the interaction between gravity and quantum theory. It is unusual to obtain a decay law from quantum mechanics without some form of approximation. That we do so in the present case is a consequence of the fact that the system is open. States are allowed to decay onto the singularity, but no accompanying emission is considered. A complete treatment of the problem as a closed system would require a quantum theory of the singularity, and such a theory does not yet exist.

The decay rates represent one feature of the quantum-mechanical description of the capture process. But, as well as decay, the quantum description of a particle falling onto the singularity of a black hole can involve a series of quantum jumps to lower energy orbits. This quantum description alters the physics of the process quite dramatically from the classical picture. As the particle undergoes a series of transitions we expect that it should radiate, which does not happen classically. What form this radiation should take (electromagnetic, gravity waves) is unclear. Also, as a transition takes place we should keep careful track of the evolution of the matter stress-energy tensor to tell us where the radiated energy is concentrated. A related problem this exposes is that we have not considered back-reaction on the gravitational field, which could alter this picture.

The quantum treatment of a particle in a gravitational field exhibits a curious antiparallelism with the electromagnetic case. In classical electrodynamics a charged particle in orbit around a point source should radiate, making atoms unstable. This problem is resolved by quantum mechanics, which predicts the existence of stable, nonradiating bound states. The reverse is true of gravitation. Classically, a particle can orbit a black hole in a geodesic outside the horizon, and such an orbit is stable. But quantum theory changes this, and states that no totally stable orbits exist, due to the finite probability of the particle finding itself inside the horizon and ending on the singularity. While the time scales involved in these decays may be of limited interest astrophysically, such processes are clearly of fundamental importance in understanding the interplay between quantum theory and gravitation.

A final point to raise here is that the spectrum of real energies derived here has a mirror image of negative energy bound states. Each of these negative energy states also has a finite lifetime. If we model the vacuum in terms of a Dirac sea of filled negative energy states, we must include the bound states as well as the free continuum. It then follows that the vacuum itself is decaying—the black hole is sucking in the vacuum. Such a loss of negative energy states is seen as a creation of positive energy modes, which could contribute to Hawking radiation. This contribution appears to have been neglected in previous calculations, which concentrate only on the scattered states [1]. It is well known in calculations of the Lamb shift, for example, that ignoring the bound states in the calculation gives the wrong answer [19]. It would be of great interest to assess the contribution played by bound states to the gravitational analog of this process.

[1] N. D. Birrell and P. C. W. Davies, *Quantum Fields in Curved Space* (Cambridge University Press, Cambridge, UK, 1982).
[2] S. Chandrasekhar, *The Mathematical Theory of Black Holes* (Oxford University Press, Oxford, 1983).
[3] R. Brout, S. Massar, R. Parentani, and P. Spindel, Phys. Rep. **260**, 329 (1995).
[4] C. J. L. Doran and A. N. Lasenby, Phys. Rev. D **66**, 024006 (2002).
[5] A. N. Lasenby and C. J. L. Doran, in *Geometric Algebra, Dirac Wavefunctions and Black Holes*, edited by P. G. Bergmann and V. de Sabbata, Advances in the Interplay Between Quantum and Gravity Physics (Kluwer, Dordrecht, 2002), pp. 251–283.
[6] C. J. L Doran and A. N. Lasenby, *Geometric Algebra for Physicists* (Cambridge University Press, Cambridge, UK, 2003).
[7] N. Deruelle and R. Ruffini, Phys. Lett. **52B**, 437 (1974).
[8] A. B. Gaina and F. G. Kochorbé, Sov. Phys. JETP **65**, 211 (1987).
[9] I. M. Ternov and A. B. Gaina, Sov. Phys. J. **31**, 157 (1988).
[10] A. B. Gaina and O. B. Zaslavskii, Classical Quantum Gravity **9**, 667 (1992).
[11] A. N. Lasenby, C. J. L. Doran, and S. F. Gull, Phil. Trans. R. Soc. A **356**, 487 (1998).
[12] M. Nakahara, *Geometry, Topology and Physics* (Adam Hilger, Bristol, 1990).
[13] *Heun's Differential Equations*, edited by A. Ronveaux (Oxford University Press, Oxford, 1995).
[14] C. J. L. Doran, A. N. Lasenby, S. Dolan, and I. Hinder, Phys. Rev. D **71**, 124020 (2005).
[15] N. Sanchez, Phys. Rev. D **16**, 937 (1977).
[16] P. Exner, *Open Quantum Systems and Feynman Integrals* (Kluwer, Dordrecht, 1985).
[17] A. Caceres and C. J. L. Doran, Phys. Rev. A **72**, 022103 (2005).
[18] C. J. L. Doran, Phys. Rev. D **61**, 067503 (2000).
[19] C. Itzykson and J-B. Zuber, *Quantum Field Theory* (McGraw-Hill, New York, 1980).